FULL PAPER

Synthesis of New DNA G-Quadruplex Constructs with Anthraquinone Insertions and Their Anticoagulant Activity

by **Alaa S. Gouda**[a])[b]), **Mahasen S. Amine**[b]), and **Erik B. Pedersen***[a])

[a]) Department of Physics, Chemistry and Pharmacy, Nucleic Acid Center, University of Southern Denmark, Campusvej 55, DK-5230 Odense M (phone: +4565502555; e-mail: erik@sdu.dk)

[b]) Department of Chemistry, Faculty of Science, Benha University, Benha, Egypt 13518

1,4-Dihydroxyanthraquinone and 1,8-dihydroxyanthraquinone were alkylated with 3-bromopropan-1-ol and subsequently transformed into the corresponding DMT protected phosphoramidite building blocks for insertion into loops of the G-quadruplex of the thrombin binding aptamer (TBA). The 1,4-disubstituted anthraquinone linker led to a significant stabilization of the G-quadruplex structure upon replacing a **T** in each of two neighboring lateral **TT** loops and a 26.2° increase in thermal melting temperature was found. CD Spectra of the modified quadruplexes confirmed anti-parallel conformations in all cases under potassium buffer conditions as previously observed for TBA. Although the majority of the anthraquinone modified TBA analogues showed a decrease in clotting times in a fibrinogen clotting assay when compared to TBA, modified aptamers containing a 1,8-disubstituted anthraquinone linker replacing $\mathbf{G_8}$ or $\mathbf{T_9}$ in the **TGT** loop showed improved anticoagulant activities. Molecular modeling studies explained the increased thermal melting temperatures of anthraquinone-modified G-quadruplexes.

Introduction. – Single-stranded guanosine-rich oligodeoxyribonucleotides have a propensity to fold into a guanine quadruplex architecture [1 – 3]. Such quadruplexes are stabilized by planar arrays of four guanines (G-tetrads) forming *Hoogsteen* H-bonds and by monovalent alkali cations such as K^+ and Na^+ ions located in the central cavity of the structure (*Fig. 1*) [4][5]. These cations play an important role in folding topology and stability of G-quadruplexes. It has also been recognized that G-quartets can adopt both intramolecular and intermolecular structures, in which single-stranded DNA is folded to provide the four strands of the guanine scaffold [6][7].

Subsequent studies indicated that putative G-quartet sequences are frequently located not only in the genome [8], but also in the 5′-untranslated regions of human mRNAs [9][10] and in transcriptome [11], including gene promoter regions [12] or gene bodies and telomeres. This provides these structures with the potential to act as regulatory elements of different processes [13][14] and cause a potent antiproliferative influence in tumor cells [15][16]. Furthermore, G-quadruplexes have been proposed to interfere with important biological processes for cellular homeostasis [17][18], such as DNA damage response activation [19 – 21], oncogene expression [22 – 26], and genomic stability [27] besides nanotechnological significance [28]. The major aim of this study is to evaluate the thermal stability of modified oligonucleotide-forming G-quadruplexes bearing new unnatural intercalators.

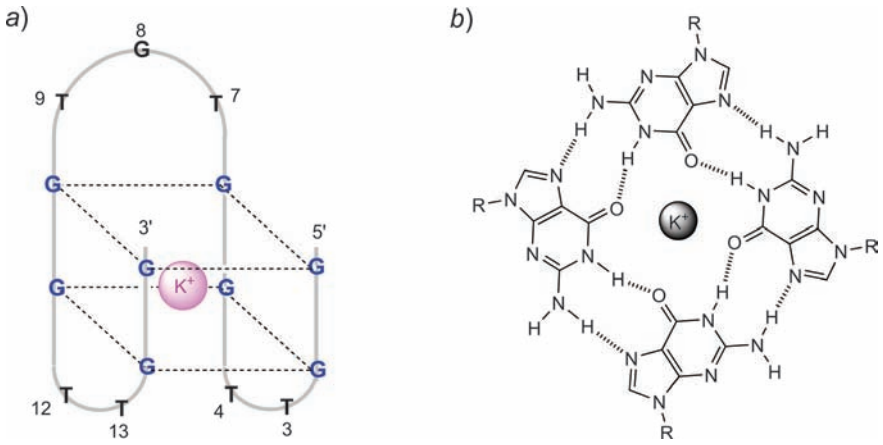

Fig. 1. *a*) *Schematic structure of the intramolecular G-quadruplex formed by TBA, b*) *the arrangement of guanine bases in the G-tetrad, shown together with a centrally placed* K^+ *metal ion.* H-Bonds are shown as dotted lines.

DOI: 10.1002/hlca.201500207

Biophysical methods have found G-quadruplexes in several oligonucleotide aptamers and G4-decoys [29]. In addition to intense speculation about the role of G-quartet formation *in vivo*, there is considerable interest in the therapeutic potential of quadruplex oligonucleotides as aptamers [2]. These are short, structured, single-stranded RNA or DNA ligands characterized by high affinity to selectively act as inhibitors of signal transduction or transcription *via* binding to particular targets, such as nucleolin or nucleolin-like protein in cancer cells [30][31]. The best-known fully characterized aptamer is a 15-mer oligonucleotide whose sequence is 5′-GGTTGGTGTGG-TTGG-3′, termed as thrombin binding DNA aptamer (TBA) [32]. It folds into a typical chair-like G-quadruplex structure containing one **TGT** groove and two lateral **TT** loops (*Fig. 1*) [33]. It binds thrombin acting as an anticoagulant agent [34]. Previous structure–activity relationship (SAR) investigations on TBA analogues containing an acyclic nucleotide, have confirmed that some loop residue, (specifically $\mathbf{T_4}$, $\mathbf{T_{13}}$, $\mathbf{G_8}$, and $\mathbf{T_9}$) have rigid positions and are crucial to preserve the G-quadruplex folding topology, whereas others ($\mathbf{T_3}$, $\mathbf{T_7}$, and $\mathbf{T_{12}}$) are more flexible moieties and involved in thrombin inhibition [35]. Here, we describe the ability of anthraquinone-modified 15-mer aptamers to inhibit thrombin-mediated coagulation.

We found this study interesting because oligonucleotides containing planar polycyclic chromophores such as stilbene [36], phenanthrene [37], pyrene [38], perylene [39], or phenanthroline [40] have the possibility to form intramolecular π-stacking interactions in aqueous solutions [41 – 43]. Anthraquinone and its derivatives are well-known intercalators that represent an interesting scaffold to develop selective and multifunctional G-quadruplex ligands [44]. They are frequently used as DNA targeting drugs [45]. Not surprisingly, conjugation of anthraquinone to oligonucleotides has served as an approach for enhancement of high affinity oligonucleotides [46]. Furthermore, the low redox potential of anthraquinone derivatives opens possibilities for charge transport through DNA [47] and electrochemical DNA sensing [48]. In addition, they behaved as photo-activated nucleases [49] and can act as molecular entities for supramolecular assemblies [50][51].

Results and Discussion. – *Synthesis of Phosphoramidite Building Blocks and Oligonucleotides.* In order to get an indication of the influence of the substitution pattern of the anthraquinone on the stability of the G-quadruplexes, we selected 1,4-dihydroxyanthraquinone (**1**) and 1,8-dihydroxyanthraquinone (**2**) for this study. The synthetic route to obtain the 1,4-disubstituted and 1,8-disubstituted anthraquinone phosphoramidites is shown in the *Scheme*. Both OH groups were alkylated by treatment with 3-bromopropan-1-ol in the presence of K_2CO_3 and KI following a similar method as described in the literature [52]. The obtained bis(3-hydroxypropoxy)-substituted anthraquinones **3** and **4** were converted into the monoprotected DMT (=dimethoxyltrityl) derivatives **5** and **6** by reaction with 4,4′-dimethoxytrityl chloride in pyridine under N_2. Subsequent phosphitylation was done under standard conditions using 2-cyanoethyl *N*,*N*-diisopropylchlorophosphoramidite ($NC(CH_2)_2OP(^iPr_2N)Cl$) in anhydrous CH_2Cl_2 under Ar to afford the phosphoramidite derivatives **7** and **8**. The attempt to use 2-cyanoethyl-*N*,*N*,*N*′,*N*′-tetraisopropylphosphordiamidite in the presence of *N*,*N*-diisopropylammonium tetrazolide as an activator in the phosphitylation reaction was unsuccessful. The DMT-protected phosphoramidites **7** and **8** were subsequently used for replacement of the corresponding monomer into oligonucleotides by using a standard procedure. The coupling efficiency was over 99% as determined by detritylation measurement. Deprotection process followed by HPLC purification yielded the oligonucleotides **ON2** – **ON18**. The correct molecular weights of all oligonucleotides were verified by matrix-assisted laser desorption/ionization time-of-flight (MALDI-TOF) mass spectrometry analysis.

Scheme. *Synthesis of Anthraquinone Intermediates and Phosphoramidite Building Blocks* **7** *and* **8**

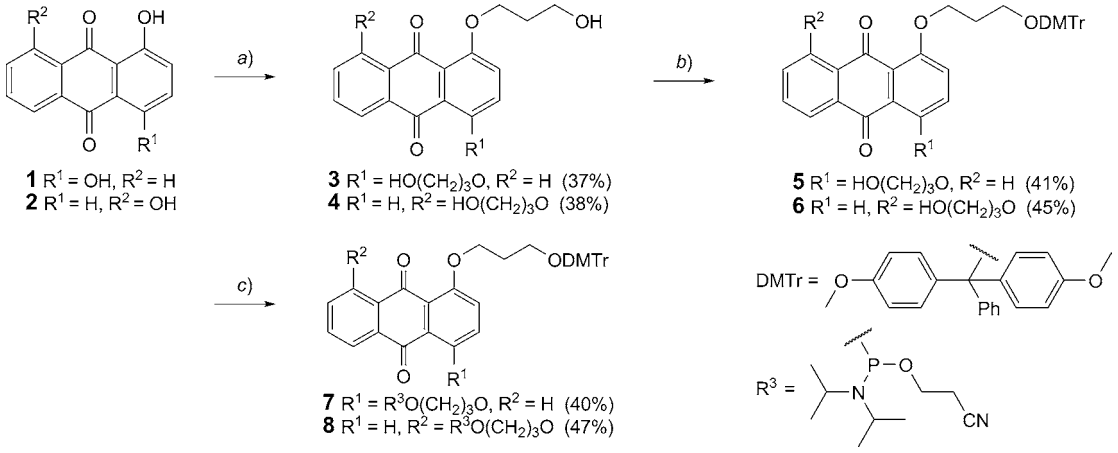

a) $Br(CH_2)_3OH$, K_2CO_3, KI, DMF, reflux, 48 h. *b*) DMTrCl, pyridine, r.t., 6 h. *c*) $NC(CH_2)_2OP(^iPr_2N)Cl$, $Et(^iPr_2)N$, CH_2Cl_2, r.t., 2 h.

Influence of Anthraquinone Building Blocks on Thermal Stability of G-Quadruplexes. The project was designed to study the effect of the two non-nucleosidic anthraquinone monomers $\mathbf{H_{14}}$ and $\mathbf{H_{18}}$ on the stability of G-quadruplexes by thermal denaturation experiments using the UV melting method at 295 nm and pH 7.5. As shown in *Table 1*, thermal stabilities were determined for oligonucleotides **ON2** – **ON8** with modifications in the **TGT** groove when compared to the wild type oligonucleotide **ON1**. For all possible replacements of one nucleotide with $\mathbf{H_{14}}$ or $\mathbf{H_{18}}$, the thermal melting (T_m) reduced in the range -2.4 to $-12.0°$. The minor change in T_m was found for replacement of $\mathbf{T_7}$, whereas replacement of $\mathbf{T_9}$ revealed the major change in T_m. In contrast, replacement of the two nucleotides sequence $\mathbf{T_7G_8}$ by $\mathbf{H_{18}}$ resulted in an increase in stability ($\Delta T_m = +4.2°$, **ON4**). However, it was a 9.0° decrease in T_m when $\mathbf{H_{14}}$ was inserted at the same position **ON8**.

According to circular dichroism (CD) spectral analysis, there seems no change in the antiparallel structures of the synthesized G-quadruplexes. Wild type **ON1** and **ON2** – **ON8** all showed positive peaks around 290 nm and negative peaks around 265 nm.

Assuming $\mathbf{H_{18}}$ suitable for replacing two nucleotide sequences, we thought it interesting to replace $\mathbf{T_3T_4}$ and/or $\mathbf{T_{12}T_{13}}$ in the lateral loops of TBA. Indeed, the T_m of modified TBA increased 8.0° upon replacement of $\mathbf{T_3T_4}$ (**ON10**) by $\mathbf{H_{18}}$ (*Table 2*). Also replacement of the $\mathbf{T_{12}T_{13}}$ loop increased T_m by 7.6° **ON11**. On the other hand, double replacement of $\mathbf{H_{18}}$ instead of the two **TT** loops reduced the increase in melting temperature to 4.0° **ON12**.

The CD spectra of **ON10** – **ON12** also showed nearly the same ellipticities around 290 nm and 265 nm as was found for **ON1**. Such data are consistent with antiparallel G-quadruplex conformations for these modifications as well.

From molecular modeling (*vide infra*), we expected a good chance to enhance the thermal stability of the TBA quadruplex by replacing single nucleotide in the lateral loops with $\mathbf{H_{14}}$. In *Table 3*, there is shown the T_m from a systematic study of replacing one nucleotide with $\mathbf{H_{14}}$ in both lateral loops. Although there is a negligible effect upon replacing the single nucleotide $\mathbf{T_4}$ or $\mathbf{T_{13}}$, there was observed substantial increases in T_m upon double replacements. The most favorable increase in T_m was observed for **ON15** when $\mathbf{T_4}$ and $\mathbf{T_{13}}$ both were replaced by $\mathbf{H_{14}}$ resulting in ΔT_m 26.2°.

This could be a result of intrastrand stacking of the anthraquinone building blocks in the two lateral loops as

Table 1. *T_m ([°]) and ΔT_m ([°]) for Melting of G-Quadruplexes Evaluated from UV Melting Curves*

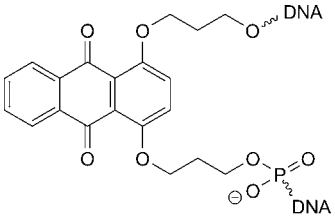

$\mathbf{H_{14}}$ (1,4-linker)

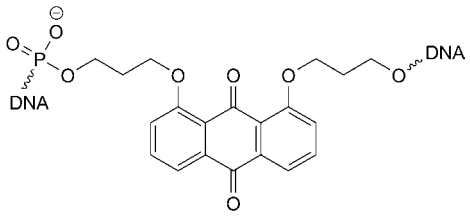

$\mathbf{H_{18}}$ (1,8-linker)

Code	Bases replaced	Sequence	T_m [°][a])	ΔT_m [°][b])
ON1	wild type	5′-GGT TGG TGT GGT TGG-3′	50.0	–
ON2	T_7	5′-GGT TGG H_{18}GT GGT TGG-3′	47.0	– 3.0
ON6	T_7	5′-GGT TGG H_{14}GT GGT TGG-3′	47.6	– 2.4
ON3	G_8	5′-GGT TGG TH_{18}T GGT TGG-3′	43.6	– 6.4
ON7	G_8	5′-GGT TGG TH_{14}T GGT TGG-3′	47.2	– 2.8
ON4	T_7G_8	5′-GGT TGG H_{18}T GGT TGG-3′	54.2	4.2
ON8	T_7G_8	5′-GGT TGG H_{14}T GGT TGG-3′	41.0	– 9.0
ON5	T_9	5′-GGT TGG TGH_{18} GGT TGG-3′	42.0	– 8.0
ON9	T_9	5′-GGT TGG TGH_{14} GGT TGG-3′	38.0	– 12.0

[a]) 4 μM of each strand at 295 nm in potassium buffer (100 mM KCl, 20 mM K_2HPO_4, and 1 mM K_2EDTA, pH = 7.5). [b]) Difference in T_m relative to wild-type **ON1**.

Table 2. *T_m ([°]) and ΔT_m ([°]) for Melting of G-Quadruplexes Evaluated from UV Melting Curves*

Code	Bases replaced	Sequence	T_m [°][a])	ΔT_m [°][b])
ON1	–	5′-GGT TGG TGT GGT TGG-3′	50.0	–
ON10	T_3T_4	5′-GGH_{18} GGT GTG GTT GG-3′	58.0	8.0
ON11	$T_{12}T_{13}$	5′-GGT TGG TGT GGH_{18} GG-3′	57.6	7.6
ON12	T_3T_4, $T_{12}T_{13}$	5′-GGH_{18} GGT GTG GH_{18}GG-3′	54.0	4.0

[a]) 4 μM of each strand at 295 nm in potassium buffer (100 mM KCl, 20 mM K_2HPO_4, and 1 mM K_2EDTA, pH = 7.5). [b]) Difference in T_m relative to wild-type **ON1**.

Table 3. T_m ([°]) *and* ΔT_m ([°]) *for Melting of G-Quadruplexes Evaluated from UV Melting Curves*

Code	Bases replaced	Sequence	T_m [°][a])	ΔT_m [°][b])
ON1	wild type	5′-GGT TGG TGT GGT TGG-3	50.0	–
ON13	T_4	5′-GGT H_{14}GG TGT GGT TGG-3′	50.0	0.0
ON14	T_{13}	5′-GGT TGG TGT GGT H_{14}GG-3′	49.8	– 0.2
ON15	T_4, T_{13}	5′-GGT H_{14}GG TGT GGT H_{14}GG-3′	76.2	26.2
ON16	T_4, T_{12}	5′-GGT H_{14}GG TGT GGH_{14} TGG-3′	60.2	10.2
ON17	T_3, T_{12}	5′-GGH_{14} TGG TGT GGH_{14} TGG-3′	68.8	18.8
ON18	T_3, T_{13}	5′-GGH_{14} TGG TGT GGT H_{14}GG-3′	59.0	9.0

[a]) 4 μM of each strand at 295 nm in potassium buffer (100 mM KCl, 20 mM K_2HPO_4, and 1 mM K_2EDTA, pH = 7.5). [b]) Difference in T_m relative to wild-type **ON1**.

described in the section about molecular modeling. For all the quadruplexes **ON13** – **ON18** an antiparallel structure is most likely according to the CD spectra with negative and positive ellipticities around 265 nm and 290 nm, respectively.

Molecular Modeling. In order to assess the ability of $\mathbf{H_{18}}$ to stack onto G-quadruplexes upon replacement of **TT** lateral loops, as well as to evaluate the variation in T_m values, we performed molecular modeling studies. A modified AMBER* force field in Macro Model 9.2 molecular modeling was utilized to generate representative low-energy structures of modified 15mer TBA. The question now is why single substitution with a **TT** loop raises the T_m values of a G-quadruplex up to 8.0° for **ON10**, while for double replacement the increase is only 4.0° for **ON12**. By replacement of one **TT** loop, intramolecular π-π* stacking interactions of $\mathbf{H_{18}}$ to the underlying G-quartet are rendered possible as shown in *Fig. 2*,*a*. However, in case of replacement of both lateral **TT** loops by $\mathbf{H_{18}}$, the two anthraquinone building blocks are not arranged in a face-to-face stacking mode. No further stabilization can be expected, since one of the two anthraquinone moieties is positioned outside the quadruplex (*Fig. 2*,*b*).

In the case of $\mathbf{H_{14}}$ for the replacement of $\mathbf{T_4}$, molecular modeling shows stacking possible between the anthraquinone moiety and the underling G-quartet as shown for **ON13** in *Fig. 3*,*a*. However, the stacking effect is not reflected in a higher melting temperature compared to the wild-type quadruplex **ON1** and one has to assume that the stacking effect on the melting temperature is counteracted by strain and/or sterical clashes within the quadruplex structure. When replacing both $\mathbf{T_3}$ and $\mathbf{T_{14}}$ with $\mathbf{H_{14}}$, the two anthraquinones stacking moieties are arranged in a face-to-face stacking mode (**ON15**, *Fig. 3*,*b*) nicely explaining the significant increase in T_m of 26.2°.

We think the two anthraquinone moieties are optimally placed for stacking in **ON15** because nearly the same stacking interaction was obtained, when the two anthraquinone units were studied alone in an unrestricted manner by molecular modeling.

Fibrinogen Clotting Inhibition by Modified Quadruplexes. It is well-known that the thrombin binding aptamer

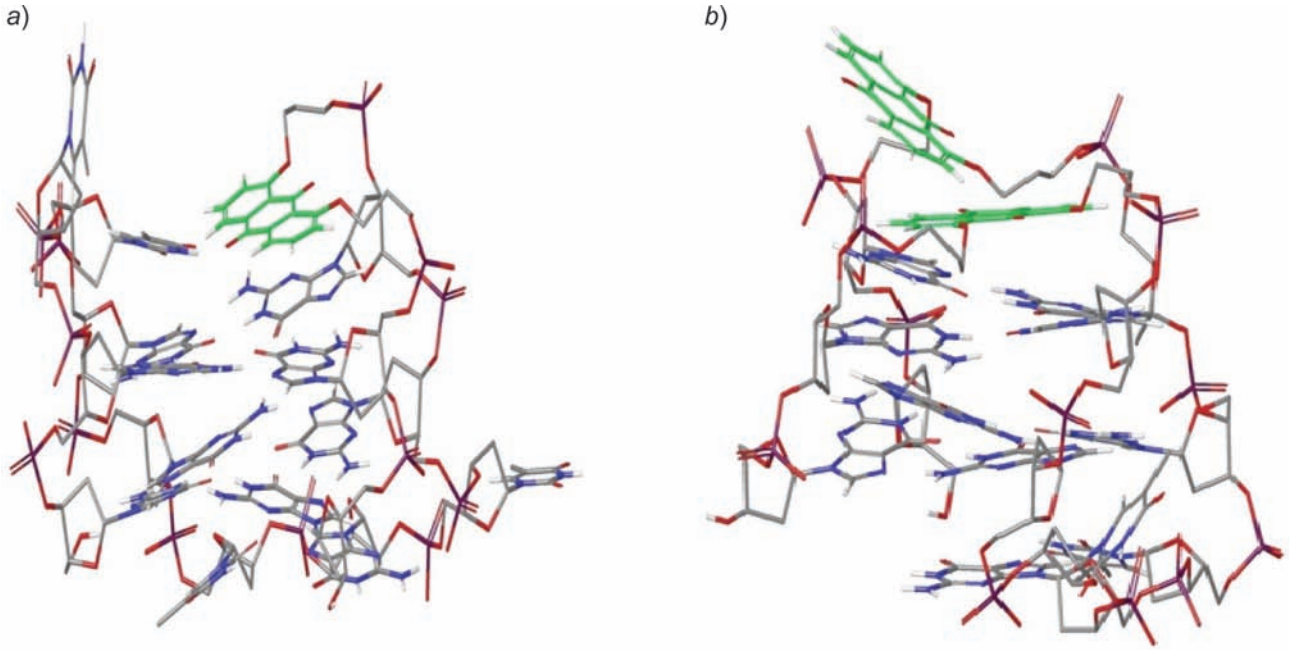

Fig. 2. *Possible conformations of a G-quadruplex containing a 1,8-anthraquinone intercalator*

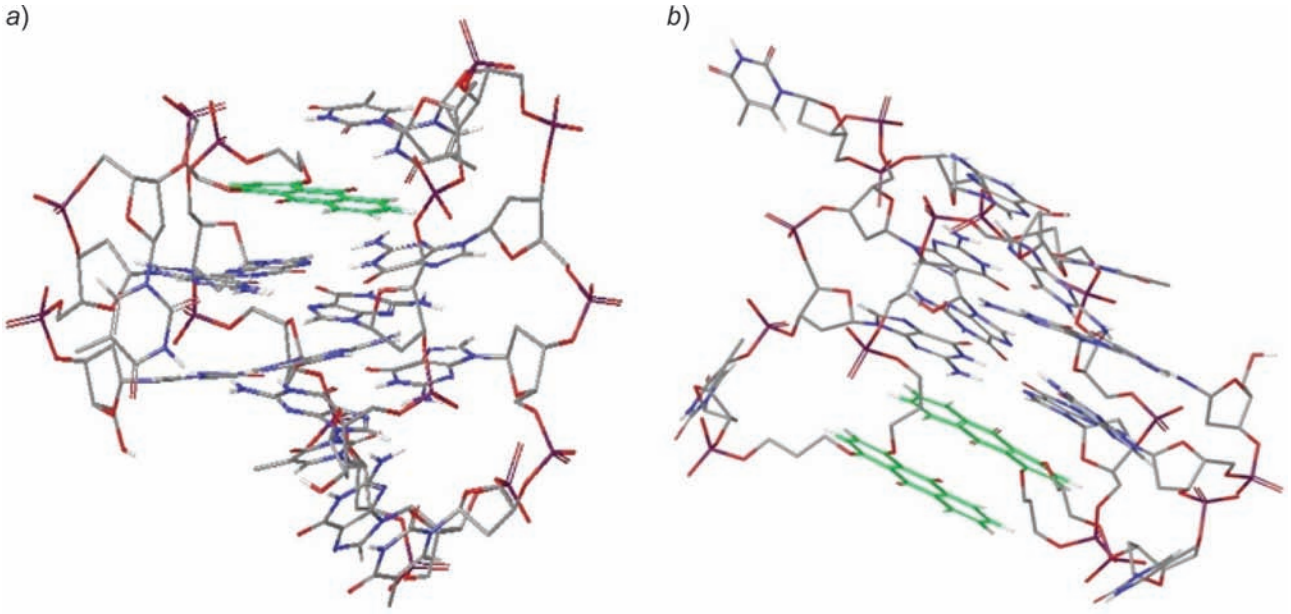

Fig. 3. *Possible conformations of G-quadruplexes containing a 1,4-anthraquinone intercalator*

(TBA) is able to bind to thrombin and thereby inhibit its enzymatic activity. The decreased activity results in prolonged clotting times for fibrinogen. The stronger the modified aptamers are able to interact with thrombin, the longer the time it takes to clot fibrinogen. We used this assay to evaluate the ability of the modified aptamers **ON2** – **ON18** in comparison to **TBA** (**ON1**) to inhibit fibrinogen clotting. The human α-thrombin-induced clotting of fibrinogen was measured spectrophotometrically, by following the increase in absorbance at 380 nm over time at 100 nM aptamer concentration. For **ON5** with replacement of $\mathbf{T_9}$ by $\mathbf{H_{18}}$ in the **TGT** loop, the clotting time was prolonged to 250 s which should be compared to **TBA** with a clotting time of 164 s. Also, **ON3** had a longer clotting time (181 s) than **TBA**. In all other cases for replacement by $\mathbf{H_{18}}$ as well as with $\mathbf{H_{14}}$ in the **TGT** loop, shorter clotting times than the one for **TBA** were recorded, although they were found substantially longer than in the absence of any inhibitor, except for **ON9** (*Fig. 4*, *a*). On the other hand, the inhibitory efficiencies of all modified sequences at the two lateral **TT** loops were lower than that of the parent **TBA** for replacement by either $\mathbf{H_{14}}$ or $\mathbf{H_{18}}$ (*Fig. 4*, *b*). In fact, in comparison with absence of inhibitor only **ON11**, **ON12**, and **ON18** showed prolonged clotting times. The best aptamer in this series was considered to be **ON12** with both **TT** loops replaced with $\mathbf{H_{18}}$. The finding that the most active aptamers were found upon replacing nucleotides in the **TGT** loop by an anthraquinone intercalator is in conformity with earlier studies where a substantial prolonged clotting time was observed when replacing $\mathbf{G_8}$ with the pyrene intercalator TINA [53].

Conclusions. – Two isomeric substituted anthraquinones $\mathbf{H_{14}}$ and $\mathbf{H_{18}}$ were synthesized and incorporated into oligodeoxynucleotides. A strong influence on thermal stability of G-quadruplexes was observed when $\mathbf{H_{14}}$ and $\mathbf{H_{18}}$ were replacing nucleotides in the loops of the TBA G-quadruplex. In the **TGT** groove, a substantial reduction in the T_m values was observed by replacement of one nucleotide, whereas an increase was observed for replacing $\mathbf{T_7G_8}$ by $\mathbf{H_{18}}$. The highest increase in thermal stability was found upon replacing $\mathbf{H_{14}}$ by a **T** in each of the two neighboring lateral **TT** loops of the G-quadruplex and the increase in T_m was found to be 26.2°. According to molecular modeling, this could be a result of a face-to-face stacking mode. In fibrinogen clotting inhibition experiments, aptamers containing $\mathbf{H_{18}}$ in the **TGT** loop region were more active than the ones containing $\mathbf{H_{14}}$. The anthraquinone derivatives described here extend the set of artificial building blocks with potential of applications for new DNA architectures.

Financial support by *Cultural Affairs & Missions Sector*, *Egyptian Ministry of Higher Education* in addition to *Biomolecular Nanoscale Engineering Center* (*Bio-NEC*), funded by the *Danish National Research Foundation*, are gratefully acknowledged.

Experimental Part

General. All reagents used were purchased from *Sigma–Aldrich* or *Fluka* and used without purification. *N,N*-Diisopropylethylamine (DIPEA), *N,N*-dimethylformamide (DMF), and pyridine were dried over 4 Å activated molecular sieves, and their dryness was determined on *Karl Fischer* titrator (< 15 ppm). Microanalysis was performed at Copenhagen University. The wild type DNA oligonucleotide, DNA phosphoramidite monomers, solid supports, and additional reagents were purchased from *Sigma–Aldrich* or *Glen Research*. TLC: *Merck Kieselgel 60* F_{254} (0.22 mm thickness, precoated aluminum plates). TLC Spots of DMT containing compounds were visualized with UV light (254 nm) as orange or dark spots when stained with 5% ethanolic H_2SO_4 soln. If compounds were sensitive to acid, the silica was pretreated with solvent containing 1% Et_3N. Column chromatography

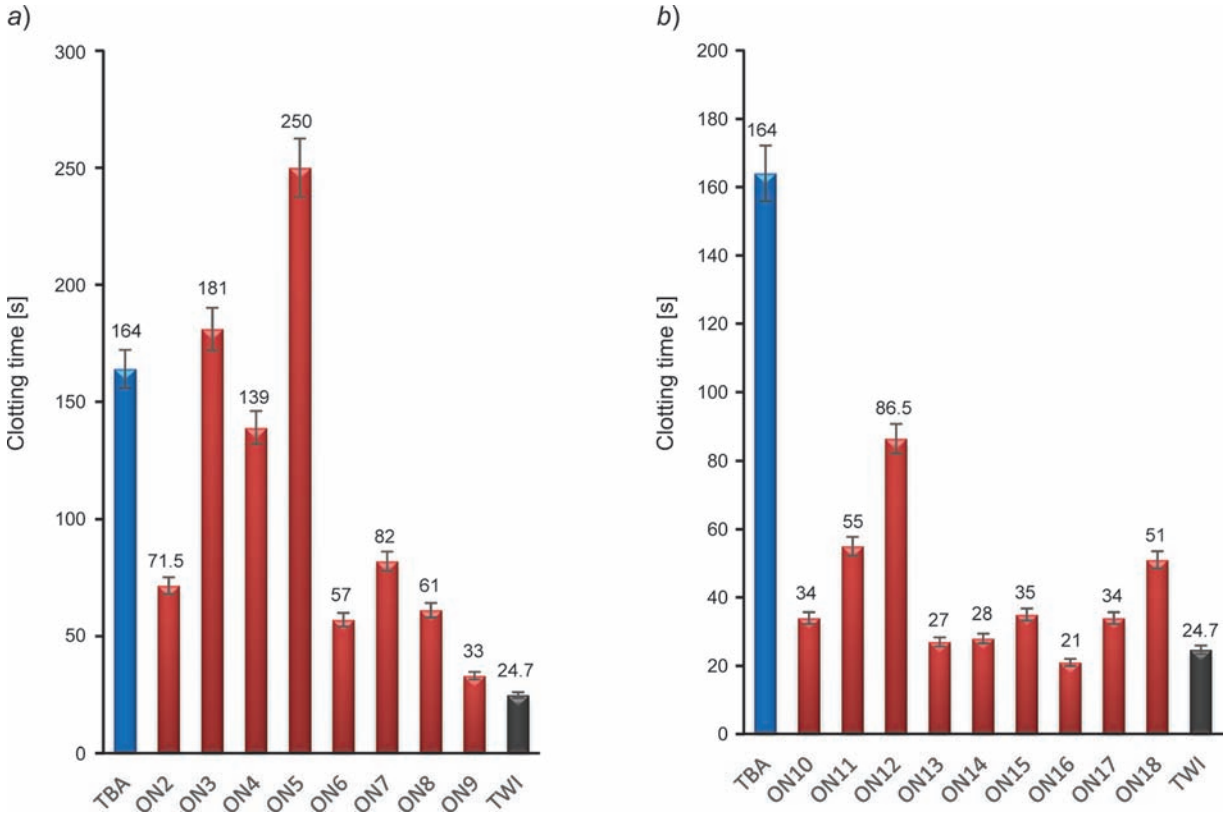

Fig. 4. *Fibrinogen clotting time* ([s]) *measured in PBS buffer in the presence of fibrinogen* ([2 mg ml^{-1}]), *thrombin* (10 NIH per ml), *and TBA/modified ONs at 100* nM *aptamer concentration.* The graphics were drawn from scattering curve data. *a*) Clotting time ([s]) for **ON1** – **ON9**, *b*) Clotting time ([s]) for **ON10** – **ON18**. TWI is thrombin without inhibitors.

(CC): *Merck Millipore* silica gel *60* (0.040 – 0.063 mm); under pressure. CH_2Cl_2 was always used freshly distilled and solvents used for CC of final phosphoramidite were distilled prior to use, while other solvents, AcOEt and petroleum ether (PE b.p. 60 – 80°), were used as received. M.p.: *Büchi* melting point apparatus; not corrected. NMR Spectra: *Bruker AVANCE III 400* spectrometer (400 MHz for ^{1}H, 101 MHz for ^{13}C, and at 162 MHz for ^{31}P); δ in ppm rel. to Me_4Si as internal standard (in $CDCl_3$: 7.26 ppm for ^{1}H and 77.0 ppm for ^{13}C; 85% aq. H_3PO_4 as an external standard with 0.00 ppm for ^{31}P-NMR), J in Hz. HR-ESI-MS: *Bruker APEX III FT-ICR* mass spectrometer using $CHCl_3$ or MeCN as solvents; in m/z. For accurate ion mass determinations, the $[M+H]^+$ or $[M+Na]^+$ ion was peak matched by calibration with NaI.

General Method for Bis(3-hydroxypropoxy)anthracene-9,10-diones (**3** *and* **4**). A soln. of dihydroxyanthraquinone (4.8 g, 20.0 mmol) **1** or **2** was dissolved in dry DMF (100 ml). K_2CO_3 (27.6 g, 200 mmol) was added to the mixture. The mixture was stirred for 2 h at 120°. 3-Bromopropan-1-ol (36.15 ml, 400 mmol) and KI (6.64 g, 40.0 mmol) were added to the mixture. The mixture was stirred at 120° for 36 h, then cooled to r.t. and concentrated *in vacuo*. 2M NaOH (100 ml) was added to the residue and the mixture was extracted with CH_2Cl_2 (3 × 250 ml). The org. phases were combined, dried (anh. Na_2SO_4), filtered and concentrated under reduced pressure. The residue was co-evaporated with toluene to afford solid products. The crude products were purified by recrystallization from toluene. The reaction progress was investigated by TLC using the eluent AcOEt.

1,4-Bis(3-hydroxypropoxy)anthracene-9,10-dione (**3**). Yield: 2.65 g (37%) as dark brown needles. R_f (AcOEt) 0.48. M.p. 130 – 132°. ^{1}H-NMR ($CDCl_3$): 2.18 (*quint.*, J = 5.5, 4 H, 2 CH_2CH_2OH); 3.99 (br. *m*, 4 H, 2 CH_2OH); 4.26 (*t*, J = 5.6, 4 H, 2 $OCH_2CH_2CH_2OH$); 4.69 (br. *s*, 2 H, 2 O*H*, D_2O exchangeable); 7.31 (*s*, 2 arom. H); 7.68 – 7.71 (*m*, 2 arom. H); 8.16 – 8.18 (*m*, 2 arom. H). ^{13}C-NMR ($CDCl_3$): 31.95 (2 CH_2CH_2OH); 61.75 (2 CH_2OH); 69.83 (2 $OCH_2CH_2CH_2OH$); 120.59; 122.11; 126.81; 133.61; 133.84; 153.42 (arom. C); 183.26 (C=O). HR-ESI-MS: 357.1321 ($[M+H]^+$, $C_{20}H_{21}O_6^+$; calc. 357.1333). Anal. calc. for $C_{20}H_{20}O_6$: C 67.41, H 5.66; found: C 67.12, H 5.63.

1,8-Bis(3-hydroxypropoxy)anthracene-9,10-dione (**4**). Yield: 2.71 g (38%) as pale green powder. R_f (AcOEt) 0.5. M.p. 169 – 171°. ^{1}H-NMR ($CDCl_3$): 2.18 (*quint.*, J = 5.5, 4 H, 2 CH_2CH_2OH); 3.97 (br. *m*, 4 H, 2 CH_2OH); 4.24 (*t*, J = 5.5, 4 H, 2 $OCH_2CH_2CH_2OH$); 4.54 (*s*, 2 H, 2 O*H*, D_2O exchangeable); 7.27 (*dd*, J = 8.4, 1.0, 2 arom. H); 7.61 (*t*, J = 7.8, 2 arom. H); 7.83 (*dd*, J = 7.7, 1.1, 2 arom. H). ^{13}C-NMR ($CDCl_3$): 32.12 (2 CH_2CH_2OH); 60.94 (2 CH_2OH); 68.87 (2 $OCH_2CH_2CH_2OH$); 119.15; 119.37; 123.46; 134.37; 134.68; 158.83 (arom. C); 183.37, 183.62 (C=O). HR-ESI-MS: 379.1144 ($[M+Na]^+$, $C_{20}H_{20}NaO_6^+$; calc. 379.1152). Anal. calc. for $C_{20}H_{20}O_6$: C 67.41, H 5.66; found: C 66.82, H 5.83.

General Method for DMT-Protection into **5** *and* **6**. The diol **3** or **4** (2.14 g, 6.0 mmol) was coevaporated with anh. pyridine (3 × 20 ml) and dissolved in dry pyridine (16 ml). 4,4′-Dimethoxytritylchloride (2.033 g, 6.0 mmol) dissolved in dry pyridine (16 ml) was added dropwise. After stirring at r.t. for 5 h under N_2, sat. aq. $NaHCO_3$ soln. was added. After extraction with CH_2Cl_2 (2 × 250 ml), drying (anh. Na_2SO_4), and concentration under reduced pressure, the product was purified by SiO_2 CC (AcOEt/PE/NEt_3 75 : 24 : 1).

1-{3-[Bis(4-methoxyphenyl)(phenyl)methoxy]propoxy}-4-(3-hydroxypropoxy)anthracene-9,10-dione (**5**). Yield: 1.621 g (41%) as dark red oil. R_f (AcOEt/PE/NEt_3 75: 24: 1) 0.57. ^{1}H-NMR ($CDCl_3$): 2.16 – 2.22 (*m*, 4 H, 2 $OCH_2CH_2CH_2O$); 3.40 (*t*, J = 5.7, 2 H, CH_2ODMT); 3.69 (*s*, 6 H, 2 *Me*O); 3.99 (br. *m*, 2 H, CH_2OH); 4.24 – 4.29 (*m*, 4 H, $OCH_2CH_2CH_2ODMT$, $OCH_2CH_2CH_2OH$); 4.74 (*s*, 1 H, O*H*); 6.74 (*d*, J = 8.7, 4 H, DMT); 7.13 (*t*, J = 7.2, 1 H of phenyl); 7.21 (*t*, J = 7.6, 2 H of phenyl); 7.30 (*m*, 6 H, 2 arom. H, 4 DMT); 7.40 (*d*, J = 7.5, 2 H of phenyl); 7.68 – 7.71 (*m*, 2 arom. H); 8.08 – 8.10 (*m*, 1 arom. H); 8.20 – 8.22 (*m*, 1 arom. H). ^{13}C-NMR ($CDCl_3$): 30.11; 32.00 (2 $OCH_2CH_2CH_2O$); 55.11 (2 MeO); 59.54 (CH_2OH); 61.97 (CH_2ODMT); 67.45;

69.96 ($OCH_2CH_2CH_2ODMT$, $OCH_2CH_2CH_2OH$); 85.89 (Ph_3CO); 112.96; 120.02; 122.33; 126.60; 127.69; 128.15; 130.04; 133.48; 134.24; 136.40; 145.24; 153.25; 153.90; 158.33 (arom. C, DMT); 182.57; 183.64 (2 C=*O*). HR-ESI-MS: 681.2430 ($[M+Na]^+$, $C_{41}H_{38}NaO_8^+$; calc. 681.2459).

1-{3-[Bis(4-methoxyphenyl)(phenyl)methoxy]propoxy}-8-(3-hydroxypropoxy)anthracene-9,10-dione (**6**). Yield: 1.787 g (45%) as yellow powder. R_f (AcOEt/PE/NEt_3 75: 24: 1) 0.70. M.p. 85 – 87°. ^{1}H-NMR ($CDCl_3$): 2.07 – 2.22 (*m*, 4 H, 2 $OCH_2CH_2CH_2O$); 3.42 (*t*, *J* = 5.5, 2 H, CH_2ODMT); 3.67 (*s*, 6 H, 2 *Me*O), 3.88 (br. *m*, 2 H, CH_2OH); 4.22 – 4.29 (*m*, 5 H, $OCH_2CH_2CH_2ODMT$, $OCH_2CH_2CH_2OH$, *OH* D_2O exchangeable); 6.71 (*d*, *J* = 8.8, 4 H, DMT); 7.10 (*t*, *J* = 7.3, 1 H of phenyl); 7.19 (*t*, *J* = 7.6, 2 H of phenyl); 7.29 (*m*, 6 H, 2 arom. H, 4 DMT); 7.39 (*d*, *J* = 7.4, 2 H of phenyl); 7.63 (*m*, 2 arom. H); 7.83 (*d*, *J* = 7.2, 1 arom. H); 7.88 (*d*, *J* = 7.2, 1 arom. H). ^{13}C-NMR ($CDCl_3$): 29.93; 31.98 (2 $OCH_2CH_2CH_2O$); 55.08 (2 *Me*O); 59.30 (CH_2OH); 61.57 (CH_2ODMT); 66.89; 69.53 ($OCH_2CH_2CH_2ODMT$, $OCH_2CH_2CH_2OH$); 85.78 (Ph_3CO); 112.89; 118.73; 119.62; 123.68; 126.51; 127.62; 128.23; 130.10; 134.00; 134.72; 136.48; 145.30; 158.27; 159.32 (arom. C, DMT); 182.62; 183.98 (2 C=O). HR-ESI-MS: 681.2455 ($[M+Na]^+$, $C_{41}H_{38}NaO_8^+$; calc.: 681.2459).

General Method for Phosphitylated Anthraquinones (**7** *and* **8**). The alcohol **5** or **6** (0.66 g, 1 mmol) was coevaporated with anh. MeCN (2 × 25 ml) and dissolved together with ethyldiisopropylamine (0.32 g, 2.53 mmol) under Ar in dry CH_2Cl_2 (12 ml). 2-Cyanoethyl diisopropylamidochloridophosphite (0.284 g, 1.2 mmol) dissolved in dry CH_2Cl_2 (6 ml) was added dropwise. The mixture was stirred at r.t. for 1 – 2 h. The resulting mixture was directly applied on a SiO_2 column for purification (AcOEt/PE/NEt_3 75 : 24 : 1). The phosphoramidites, especially the 1,4-isomer, are sensitive to moisture and light, and they were immediately used for DNA synthesis.

3-[(4-{3-[Bis(4-methoxyphenyl)(phenyl)methoxy]propoxy}-9,10-dioxo-9,10-dihydroanthracen-1-yl)oxy]propyl 2-Cyanoethyl Dipropan-2-ylphosphoramidoite (**7**). Yield: 0.34 g (40%) as brown semi-solid. R_f (AcOEt/PE/NEt_3 75 : 24 : 1) 0.63. ^{1}H-NMR ($CDCl_3$): 1.21 – 1.23 (*m*, 12 H, 4 Me); 2.17 – 2.21 (*m*, 4 H, $OCH_2CH_2CH_2OP$, $OCH_2CH_2CH_2OCPh_3$); 2.30 (*t*, *J* = 6.0, 2 H, CH_2CN); 2.71 – 2.75 (*m*, 2 H, 2 NCH); 3.38 – 3.48 (*m*, 6 H, $CH_2CH_2CH_2OP$, CH_2OCPh_3, $NCCH_2CH_2OP$); 3.70 (*s*, 6 H, 2 MeO); 4.23 – 4.27 (*m*, 4 H, $OCH_2CH_2CH_2OP$, $OCH_2CH_2CH_2OCPh_3$); 6.74 (*d*, *J* = 8.9, 4 H, DMT); 7.13 (*t*, *J* = 7.3, 1 H of phenyl); 7.21 (*t*, *J* = 7.6, 2 H of phenyl); 7.26 – 7.32 (*m*, 6 H, 2 arom. H, 4 H of DMT); 7.40 (*d*, *J* = 7.9, 2 H of phenyl); 7.69 – 7.71 (*m*, 2 arom. H); 8.08 – 8.11 (*m*, 1 arom. H); 8.14 – 8.16 (*m*, 1 arom. H). ^{13}C-NMR ($CDCl_3$): 17.17; 17.97 ($OCH_2CH_2CH_2OP$, $OCH_2CH_2CH_2OCPh_3$); 20.65 (4 Me); 28.22 (CH_2CN); 44.34 (2 NCH); 53.23 (2 MeO); 57.69; 58.15; 60.99 ($CH_2CH_2CH_2OP$, CH_2OCPh_3, $NCCH_2CH_2OP$); 64.74; 65.50 ($OCH_2CH_2CH_2OP$, $OCH_2CH_2CH_2OCPh_3$); 84.00 (Ph_3CO); 111.08; 114.50; 119.91; 121;24; 124.71; 125.81; 126.28; 128.16; 131.24; 132.41; 134.54; 143.37; 151.44; 152.15; 156.44 (arom. C, DMT); 180.85; 181.19 (2 C=O). ^{31}P-NMR ($CDCl_3$): 147.80. HR-ESI-MS: 859.3678 ($[M+H]^+$, $C_{50}H_{56}N_2O_9P^+$; calc. 859.3718).

3-[(8-{3-[Bis(4-methoxyphenyl)(phenyl)methoxy]propoxy}-9,10-dioxo-9,10-dihydroanthracen-1-yl)oxy]propyl 2-Cyanoethyl Dipropan-2-ylphosphoramidoite (**8**). Yield: 0.41 g (47%) as dark yellow powder. R_f (AcOEt/PE/NEt_3 75: 24: 1) 0.73. M.p. 72 – 74°. ^{1}H-NMR ($CDCl_3$): 1.12 – 1.17 (*m*, 12 H, 4 Me); 2.12 – 2.22 (*m*, 4 H, $OCH_2CH_2CH_2OP$, $OCH_2CH_2CH_2OCPh_3$); 2.57 (*t*, *J* = 6.4, 2 H, CH_2CN); 3.37 (*t*, *J* = 5.6, 2 H, $NCCH_2CH_2OP$); 3.52 – 3.63 (*m*, 2 H, 2 NCH); 3.70 (*s*, 6 H, 2 MeO); 3.75 – 3.97 (*m*, 4 H, $CH_2CH_2CH_2OP$, CH_2OCPh_3); 4.22, 4.28 (2*t*, *J* = 6.2, 6.5, 4 H, $OCH_2CH_2CH_2OP$, $OCH_2CH_2CH_2OCPh_3$); 6.74 (*d*, *J* = 8.8, 4 H of DMT); 7.13 (*t*, *J* = 7.2, 1 H of phenyl); 7.22 (*t*, *J* = 7.6, 2 H of phenyl); 7.26 – 7.32 (*m*, 6 H, 2 arom. H, 4 *H* of DMT); 7.41 (*d*, *J* = 7.5, 2 H of phenyl); 7.56 – 7.63 (*m*, 2 arom. H); 7.83 (*dd*, *J* = 7.3, 3.8, 2 arom. H). ^{13}C-NMR ($CDCl_3$): 20.38 (4 *Me*); 24.57 (CH_2CN); 29.71; 31.28 ($OCH_2CH_2CH_2OP$, $OCH_2CH_2CH_2OCPh_3$); 38.18 ($NCCH_2CH_2OP$); 43.00 (2 NCH); 55.12 (2 MeO); 58.42; 59.63 ($CH_2CH_2CH_2OP$, CH_2OCPh_3); 66.47; 67.10 ($OCH_2CH_2CH_2OP$, $OCH_2CH_2CH_2OCPh_3$); 85.91 (Ph_3CO); 112.99; 117.65; 118.99; 119.72; 124.44; 126.62; 127.71; 128.17; 130.02; 133.58; 134.82; 136.40; 145.20; 158.35; 158.83 (arom. C, DMT); 181.77; 184.22 (2 C=O). ^{31}P-NMR ($CDCl_3$): 147.79. HR-ESI-MS: 881.3537 ($[M+Na]^+$, $C_{50}H_{55}N_2NaO_9P^+$; calc. 881.3522).

Oligonucleotide Synthesis and Purification. Oligodeoxynucleotide synthesis was carried out on a *PerSeptive Biosystems expedite 8909* automated DNA/RNA synthesizer in 0.2 μmol scale on 500 Å (CPG support). A standard cycle protocol was applied for phosphoramidite monomers **7** and **8** using 5-[3,5-bis(trifluoromethyl)phenyl]-1*H*-tetrazole (0.25M, in dry MeCN) as an activator, followed by incorporation *via* hand-coupling into the growing oligonucleotides chain during extended coupling time (15 min). Stepwise coupling efficiencies, determined by the absorbance of trityl cation at 495 nm on UV/VIS spectrophotometer, were > 99.0% for the synthesized phosphoramidites. Removal of nucleobase protecting groups and cleavage from solid support were carried out under standard conditions (1 ml of 32% aq. ammonia, 12 h at 55°). The resulting oligonucleotides (**ON2**, **ON6**, **ON16** – **ON18**) were purified by DMTr-ON reversed phase HPLC (RP-HPLC) using the *Waters system 600* equipped with a *XBridge OST C18*-column (19 × 1000 mm, 5 μm + precolumn: *XBridge* 10 × 10 mm, 5 μm; temp. column oven: 50°). Elution was performed starting with an isocratic hold of buffer *A* for 2 min followed by a linear gradient to 70% buffer *B* over 17 min at a flow rate of 5 ml/min (Buffer *A:* 0.05M triethylammonium acetate in *Milli-Q* water, pH 7.4; Buffer *B:* 75% *Me*CN/25% Buffer *A*). **ON1**, **ON3** – **ON5**, **ON7** – **ON9**, **ON11**, **ON14**, **ON15** were used without RP-HPLC purification. **ON10**, **ON12** and **ON13** seemed to be pure enough and were initially precipitated without purification, but a pureness of less than 80% was observed after precipitation. Therefore, they were purified by anion-exchange HPLC (IE-HPLC) using the *DIONEX Ultimate 3000* system equipped with a *DNAPac PA100* semi-prep. column (13 μm, 250 mm × 9 mm) heated to 60°. Elution was performed with an isocratic hold of buffer *B* (10%), starting from 2 min hold on 2% Buffer *A* in *Milli-Q* water (solvent *A*), followed by a linear gradient to 25% buffer *A* in 20 min at a flow rate of 1.0 ml/min (buffer *A:* 1.0M $NaClO_4$; buffer *B:* 0.25M TrisCl, pH 8.0; solvent *A: Milli-Q* water). After IE-HPLC purification, the three oligonucleotides were desalted using *NAP™-10* column (*illustra™*, *GE Healthcare*, prepacked with *Sephadex™ G-25* DNA-grade resin, input sample volume up to 1 ml) according to the manufacturer's instructions.

After removing solvents under N_2 flow, oligonucleotides were detrityled by treatment with 100 μl of 80% aq. soln. of AcOH for 30 min, 100 μl double filtered H_2O, then quenched or desalted with an aq. soln. of AcONa (3M, 15 μl) and $NaClO_4$ (5M, 15 μl) followed by cold acetone (1 ml). The resulting suspension was stored at – 20° for 1 h. After centrifugation (13000 rpm, 10 min, 4°), the supernatant was removed and the pellet further washed with cold acetone (2 × 1 ml), dried for 30 min under N_2 flow, and dissolved in *MilliQ* water (1000 μl). The composition of the oligonucleotide was verified by MALDI-TOF (Matrix-assisted laser desorption/ionization-time of flight) analysis on a *Bruker Daltonics Microflex LT* (MALDI-LIFT system) MS instrument in ES^+ mode with HPA-matrix (10 mg 3-hydroxypicolinic acid in 50 mM ammonium citrate/70% MeCN) matrix. ODN found *m*/*z* (calc. *m*/*z*): **ON2** 4839.8 (4839.2), **ON3** 4814.7 (4814.2), **ON4** 4510.3 (4510.2), **ON5** 4839.4 (4839.2), **ON6** 4839.4 (4839.2), **ON7** 4814.4 (4814.2), **ON8** 4810.3 (4810.2), **ON9** 4839.8 (4839.2), **ON10** 4535.6 (4535.0), **ON11** 4535.9 (4535.0), **ON12** 4343.2 (4344.0), **ON13** 4839.9 (4839.2), **ON14** 4840.1 (4839.2), **ON15** 4952.8 (4952.4), **ON16** 4953.8 (4952.4), **ON17** 4952.8 (4952.4), **ON18** 4952.1 (4952.4). The purity of the final oligodeoxynucleotides was more than 90%, recorded by analytical IE-HPLC traces on a *Merck Hitachi La-Chrom* system equipped with a *DNAPac PA100* analytical column (13 μm, 250 mm × 4 mm) heated to 60°. Elution was performed with an isocratic hold of buffer *B* (10%), starting from 2 min hold on 2% Buffer *A* in *Milli-Q* water (solvent A), followed by a linear gradient to 30% buffer *A* in 23 min at a flow rate of 1.1 ml/min (buffer *A:* 1.0M $NaClO_4$; buffer B: 0.25M *Tris*-Cl, pH 8.0; solvent A: *Milli-Q* water).

Thermal Denaturation Studies of G-Quadruplexes. Concentrations of ONs were determined by UV at 260 nm, assuming identical molar absorptivities for unmodified DNA nucleotides. Extinction coefficients [54] were determined for the two isomeric anthraquinone moieties ($\varepsilon =$ 9.60, 8.36 $\mathbf{OD}_{260}$/μmol for $\mathbf{H_{14}}$ and $\mathbf{H_{18}}$, resp.) after measuring the absorbance averages of three measurements for each linker. Melting temp. measurements were performed on a *Perkin–Elmer Lambda 35* UV/VIS spectrometer fitted with a PTP-6 peltier temperature programmer using quartz optical cuvettes with a path length of 10.0 mm. The synthesized oligonucleotides (4 μM of each strand) were mixed with potassium buffer conditions 100 mM KCl, 20 m K_2HPO_4, and 1 mM K_2EDTA at pH 7.5 to furnish G-quadruplex forming oligonucleotides. The resulting mixtures were heated to 90° (15 min) then cooled down gradually to the starting temp. of the experiment 15°, and then were kept at this temp. for 120 min. The thermal denaturation temps. (T_m [°]) were determined as the maximum of the first derivative plots of the smoothed melting curves obtained by absorbance at 295 nm against increasing temp. (gradient 0.5°/min) (A_{295} *vs.* temp.) programmed by a *Peltier* temp. controller. All melting temps. are within the uncertainly ± 0.5° as determined by repetitive experiments and T_m values were calculated using UV-WinLab software, taking an average of the two melting curves.

Circular Dichroism Spectra. Circular dichroism spectra were collected on a *Jasco J-600A* spectropolarimeter using 1 ml quartz cuvettes with 5-mm path length. Oligonucleotides (4 μM) were dissolved in a buffer containing 100 mM KCl and 20 mM K_2HPO_4, and 1 mM K_2EDTA at pH 7.5. All samples were annealed for 2 min at 90° and slowly cooled to r.t. before data collection. The measurements were performed at 10° in the 200 – 400 nm wavelength range. The buffer spectrum was subtracted from the sample spectra. The spectra were smoothened in Microcal Origin 6.0 using a *Savitzky–Golay* filter.

Molecular Modelling. Molecular modelling was performed with Maestro v9.2 from *Schrödinger*. All calculations were conducted with AMBER* force field [55] and the GB/SA water model [56] as implemented by MacroModel. Extended cut-offs were used for non-bonded interactions (*van der Waals* 8 Å and electrostatics 20 Å). The molecular dynamic simulations were performed with stochastic dynamics, a SHAKE algorithm to constrain bonds to H-atoms, time step of 1.5 fs, and simulation temp. of 300 K. Simulation for 0.5 ns with an equilibration time of 150 ps generated 250 individual structures, which were minimized using the PRCG method [57] with maximum iterations 5000 and convergence threshold of 0.05 kJ/mol. The starting structures were generated using Protein Data Bank (PDB) code (4DII accession number), followed by incorporation of the anthraquinone monomer.

Fibrinogen Clotting Time. The fibrinogen clotting times were measured spectrophotometrically [58]. ONs were incubated for 1 min in UV-spectrometer at 37° in 500 μl of phosphate buffer saline PBS (*Sigma–Aldrich*, P4417, 1 tablet of PBS per 100 ml of deionized H_2O) containing 2.0 mg ml^{-1} of fibrinogen (fibrinogen from human plasma, F 3879, *Sigma–Aldrich*) and diluted to 1 ml total volume with *MilliQ* water. The soln. thoroughly was mixed on the vortex mixer and transferred into a PMMA semi-micro cuvette (*Brandtech*, 759086D). 100 μl of human thrombin (10 NIH units per ml, from human plasma, *Sigma–Aldrich*, T8885, human thrombin suitable for the thrombin time tests) was then added to the soln. containing the fibrinogen and the aptamers. The time required for fibrin polymerization was determined from a UV scattering curve (380 nm), recorded over time in the presence of each ONs. Each curve was determined in triplicate at 100 nM aptamer concentration. Clotting time values (mean ± SE) were derived from the time where the 50% of the final absorbance was observed as the midpoint of each scattering curve. The 15-mer 5′-GGTTGGTGTGGTTGG-3′ was used as the positive control. In the absence of any inhibitors, the clotting time value was 24.7 ± 1.0 s.

REFERENCES

[1] S. Burge, G. N. Parkinson, P. Hazel, A. K. Todd, S. Neidle, *Nucleic Acids Res.* **2006**, *34*, 5402.
[2] V. Đapić, V. Abdomerović, R. Marrington, J. Peberdy, A. Rodger, J. O. Trent, P. J. Bates, *Nucleic Acids Res.* **2003**, *31*, 2097.
[3] M. L. Bochman, K. Paeschke, V. A. Zakian, *Nat. Rev. Genet.* **2012**, *13*, 770.
[4] I. R. Krauss, A. Merlino, A. Randazzo, E. Novellino, L. Mazzarella, F. Sica, *Nucleic Acids Res.* **2012**, *40*, 8119.
[5] C. Percivalle, C. Sissi, M. L. Greco, C. Musetti, A. Mariani, A. Artese, G. Costa, M. L. Perrore, S. Alcaro, M. Freccero, *Org. Biomol. Chem.* **2014**, *12*, 3744.
[6] O. Doluca, J. M. Withers, V. V. Fililchev, *Chem. Rev.* **2013**, *113*, 3044.
[7] A. Siddiqui-Jain, C. Grand, D. Bearss, L. Hurley, *Proc. Natl. Acad. Sci. U.S.A.* **2002**, *99*, 11593.
[8] J. L. Huppert, S. Balasubramanian, *Nucl. Acids Res.* **2007**, *35*, 406.
[9] S. Nagatoishi, N. Isono, K. Tsumoto, N. Sugimoto, *BioChimie* **2011**, *93*, 2311.
[10] S. Kumari, A. Bugaut, J. L. Huppert, S. Balasubramanian, *Nat. Chem. Biol.* **2007**, *3*, 218.
[11] J. L. Huppert, A. Bugaut, S. Kumari, S. Balasubramanian, *Nucl. Acids Res.* **2008**, *36*, 6260.
[12] S. Balasubramanian, L. H. Hurley, S. Neidle, *Nat. Rev. Drug Discovery* **2011**, *10*, 261.
[13] S. Cogoi, A. E. Shchekotikhin, A. Membrino, Y. B. Sinkevich, L. E. Xodo, *J. Med. Chem.* **2013**, *56*, 2764.
[14] S. Neidle, G. Parkinson, *Nat. Rev. Drug Discovery* **2002**, *1*, 383.
[15] E. W. Choi, L. V. Nayak, P. J. Bates, *Nucl. Acids Res.* **2010**, *38*, 1623.
[16] A. Membrino, S. Cogoi, E. B. Pedersen, L. E. Xodo, *PLoS ONE* **2011**, *6*, e24421.
[17] E. B. Pedersen, J. T. Nielsen, C. Nielsen, V. V. Filichev, *Nucl. Acids Res.* **2011**, *39*, 2470.
[18] S. Cogoi, S. Zorzet, V. Rapozzi, I. Géci, E. B. Pedersen, L. E. Xodo, *Nucl. Acids Res.* **2013**, *41*, 4049.
[19] R. Rodriguez, S. Muller, J. A. Yeoman, C. Trentesaux, J. Riou, S. Balasubramanian, *J. Am. Chem. Soc.* **2008**, *130*, 15758.
[20] R. Rodriguez, K. M. Miller, J. V. Forment, C. R. Bradshaw, M. Nikan, S. Britton, T. Oelschlaegel, B. Xhemalce, S. Balasubramanian, S. Jackson, *Nat. Chem. Biol.* **2012**, *8*, 301.
[21] C. Douarre, X. Mergui, A. Sidibe, D. Gomez, P. Alberti, P. Mailliet, C. Trentesaux, J. Riou, *Nucl. Acids Res.* **2013**, *41*, 3588.
[22] T. A. Brookes, L. H. Hurley, *Nat. Rev. Cancer* **2009**, *9*, 849.
[23] S. Cogoi, A. E. Shchekotikhin, L. E. Xodo, *Nucl. Acids Res.* **2014**, *42*, 8379.
[24] T. A. Brooks, L. H. Hurley, *Genes Cancer* **2010**, *1*, 641.
[25] M. Bejugam, S. Sewitz, P. S. Shirude, R. Rodriguez, R. Shahid, *J. Am. Chem. Soc.* **2007**, *129*, 12926.
[26] A. Bugaut, S. Balasubramanian, *Nucl. Acids Res.* **2012**, *40*, 4727.
[27] K. Paeschke, M. L. Bochman, P. D. Garcia, P. Cejka, K. L. Friedman, S. C. Kowalczykowski, V. A. Zakian, *Nature* **2013**, *497*, 458.
[28] X. Liu, T. Zhou, Y. Wang, M. T. T. Ng, W. Xu, T. Li, *Chem. Commun.* **2008**, 380.
[29] M. Scuotto, M. Persico, M. Bucci, V. Vellecco, N. Borbone, E. Morelli, G. Oliviero, E. Novellino, G. Piccialli, G. Cirino, M. Varra, C. Fattorusso, L. Mayol, *Org. Biomol. Chem.* **2014**, *12*, 5235.
[30] H. W. McMicken, P. J. Bates, Y. Chen, *Cancer Gene Ther.* **2003**, *10*, 867.
[31] P. J. Bates, J. B. Kahlon, S. D. Thomas, J. O. Trent, D. M. Miller, *J. Biol. Chem.* **1999**, *274*, 26369.
[32] J. A. Kelly, J. Feigon, T. O. Yeates, *J. Mol. Biol.* **1996**, *256*, 417.
[33] L. C. Bock, L. C. Griffin, J. A. Latham, E. H. Vermaas, J. J. Toole, *Nature* **1992**, *355*, 564.

[34] W. X. Li, A. V. Kaplan, G. W. Grant, J. J. Toole, L. L. K. Leung, *Blood* **1994**, *83*, 677.
[35] A. Virgilio, L. Petraccone, M. Scuotto, V. Vellecco, M. Bucci, L. Mayol, M. Varra, V. Esposito, A. Galeone, *ChemBioChem* **2014**, *15*, 2427.
[36] F. D. Lewis, Y. S. Wu, X. Y. Liu, *J. Am. Chem. Soc.* **2002**, *124*, 12165.
[37] S. M. Langenegger, R. Häner, *ChemBioChem.* **2005**, *6*, 2149.
[38] V. V. Filichev, M. C. Nielsen, N. Bomholt, C. H. Jessen, E. B. Pedersen, *Angew. Chem, Int. Ed.* **2006**, *45*, 5311.
[39] F. Lewis, L. G. Zhang, X. B. Zuo, *J. Am. Chem. Soc.* **2005**, *127*, 10002.
[40] S. M. Langenegger, R. Häner, *ChemBioChem* **2005**, *6*, 848.
[41] V. V. Filichev, E. B. Pedersen, 'Wiley Encyclopedia of Chemical Biology', 2009, Vol. 1, p. 493.
[42] K. M. Guckian, B. A. Schweitzer, R.-F. Ren, C. J. Sheils, D. C. Tahmassebi, E. T. Kool, *J. Am. Chem. Soc.* **2000**, *122*, 2213.
[43] C. B. Nielsen, M. Petersen, E. B. Pedersen, P. E. Hansen, U. B. Christensen, *Bioconjug. Chem.* **2004**, *15*, 260.
[44] N. Bouquin, V. L. Malinovskii, R. Häner, *Eur. J. Org. Chem.* **2008**, 2213.
[45] T. Ndlebe, G. B. Schuster, *Org. Biomol. Chem.* **2006**, *4*, 4015.
[46] M. Sato, T. Moriguchi, K. Shinozuka, *Bioorg. Med. Chem. Lett.* **2004**, *14*, 1305.
[47] F. W. Shao, K. Augustyn, J. K. Barton, *J. Am. Chem. Soc.* **2005**, *127*, 17445.
[48] S. D. Wettig, G. A. Bare, R. J. S. Skinner, J. S. Lee, *Nano Lett.* **2003**, *3*, 617.
[49] D. T. Breslin, G. B. Schuster, *J. Am. Chem. Soc.* **1996**, *118*, 2311.
[50] Z. Dzolic, M. Cametti, A. D. Cort, L. Mandolini, M. Zinic, *Chem. Commun.* **2007**, *34*, 3535.
[51] E. T. Kool, J. C. Morales, K. M. Guckian, *Angew. Chem., Int. Ed.* **2000**, *39*, 990.
[52] J. A. Valderrama, H. Leiva, R. Tapia, *Synth. Commun.* **2000**, *30*, 737.
[53] F. Rhrbach, M. I. Fatthalla, T. Kupper, B. Pötzsh, J. Müller, M. Petersen, E. B. Pedersen, G. Mayer, *ChemBioChem* **2012**, 13, 631.
[54] M. J. Cavaluzzi, P. N. Borer, *Nucleic Acids Res.* **2004**, *32* (1), e13.
[55] a) S. J. Weiner, P. A. Kollman, D. A. Case, U. C. Singh, C. Ghio, G. Alagona, S. Profeta, P. Weiner, *J. Am. Chem. Soc.* **1984**, *106*, 765; b) S. J. Weiner, P. A. Kollman, D. T. Nyguyen, D. A. Case, *J. Comput. Chem.* **1986**, *7*, 230.
[56] W. C. Still, A. Tempczyk, R. C. Hawlay, T. Hendrickson, *J. Am. Chem. Soc.* **1990**, *112*, 6127.
[57] E. Polak, G. Ribière, 'Rev. Francaise Informat Recherche Operationelle', 1969, Vol. 16, p. 35.
[58] Y. R. De Cristofaro, E. Di Cera, *J. Protein Chem.* **1991**, *10*, 455.

Received August 6, 2015
Accepted September 23, 2015

